

# Non-Abelian anyons in a periodically-driven Abelian model

Francesco Petiziol

*Technische Universität Berlin, Institut für Theoretische Physik, Hardenbergstraße 36, 10623 Berlin*

We show that non-Abelian anyons can emerge from an Abelian topologically-ordered model subject to time-periodic driving, with the specific example of Ising anyons in a driven toric-code model. The toric code possesses fermionic and bosonic quasiparticles which are mutual semions, namely they see each other as  $\pi$  fluxes. The Floquet modulation addresses the fermionic quasiparticles only and is designed to induce a topologically non-trivial band structure, realizing drive-assisted  $p + ip$  pairing in the high-frequency regime. As a result, the fermions fractionalize into Floquet-Majorana zero modes hosted by the bosonic quasiparticles, which then develop non-Abelian character. These properties are analyzed through high-frequency expansions in a quasiparticle picture and, numerically, via computation of the exact quasienergy spectra and of the non-Abelian exchange phases. Our findings shed light on the nonequilibrium physics of driven topologically-ordered quantum matter and may facilitate the observation of non-Abelian behaviour in engineered quantum systems.

Quasiparticles with anyon quantum statistics are predicted to appear as gapped excitations in topologically-ordered quantum phases of matter, such as fractional quantum Hall and spin liquids [1, 2]. Braiding anyons of Abelian type can change the many-body wavefunction by a phase factor. Braiding non-Abelian anyons, instead, can induce a unitary transformation in a topologically-protected degenerate ground-state subspace, enabling fault-tolerant quantum computation [1, 3]. Although realizing and controlling non-Abelian topological order in experiments remains elusive, the observation of Abelian anyons has been recently attained in engineered quantum systems, ranging from ultracold atoms in optical lattices [4, 5] to Rydberg atom arrays [6] and superconducting circuits [7]. This progress strongly motivates the study of topologically-ordered phases out of equilibrium, such as subject to external control, which may both provide a stepping stone towards non-Abelian physics [8–11] and unveil novel effects, with first examples given by radical chiral Floquet phases [12, 13] and fractionalized prethermalization [14].

Here we show that time-periodic driving can effectively turn an Abelian topologically-ordered model into a non-Abelian one. This is demonstrated with the example of Kitaev’s toric code [3], the paradigmatic  $\mathbb{Z}_2$  spin liquid [2]: under Floquet high-frequency modulation, the system develops non-Abelian Ising anyons, otherwise predicted in  $p + ip$  topological superconductors [15], Kitaev’s honeycomb model (with a Haldane mass) [8] and the Pfaffian fractional-quantum-Hall state [16]. The toric code hosts bosonic ( $\mathbb{Z}_2$  vortex) and fermionic ( $\mathbb{Z}_2$  spinon) quasiparticle excitations behaving like mutual semions, namely seeing each other as  $\pi$  fluxes. We construct a local Floquet drive, addressing the fermion quasiparticles, which attributes them a topological band structure in the high-frequency regime, effectively forcing them into a  $p + ip$  superconducting phase. In the topological phase, attained at appropriate driving amplitude and frequency, the fermions fractionalize into Floquet-Majorana modes localized at the bosonic  $\mathbb{Z}_2$  vortices, which then acquire

non-Abelian character. This is substantiated by analytical analyses based on high-frequency expansions and numerical determination of the quasienergy spectra and of the vortex exchange phases. Our results shed light on the properties of nonequilibrium interacting topological phases and establish Floquet driving as a potential bridge between them. Moreover, they pave the way towards the development of novel protocols to Floquet-engineer non-Abelian anyons building on the control of Abelian phases recently attained [6] or predicted [17–19].

*The driven toric code model.* The Abelian toric-code model [3, 20] describes two-level systems (spins) situated on the bonds of a square  $L \times L$  lattice [Fig. 1(a)], with  $L$  even hereafter, and ruled by the Hamiltonian

$$\hat{H}_{\text{tc}} = -\frac{g}{2} \sum_v \hat{A}_v - \frac{g}{2} \sum_p \hat{B}_p . \quad (1)$$

The labels  $p$  and  $v$  denote plaquettes and vertices on the lattice,  $g$  is a coupling constant,  $\hat{A}_v = \prod_{i \in v} \hat{X}_i$  and  $\hat{B}_p = \prod_{i \in p} \hat{Z}_i$  are four-spin interactions and  $\hat{X}_i, \hat{Y}_i, \hat{Z}_i$  are Pauli matrices pertaining to the  $i$ th spin. When convenient, we will also interpret  $p = (p_x, p_y)$  and  $v = (v_x, v_y)$  as coordinates of two separate plaquette and vertex lattices, respectively, both with lattice vectors  $x = (1, 0)$  and  $y = (0, 1)$ . All four-spin operators composing  $\hat{H}_{\text{tc}}$  commute with each other,  $[\hat{A}_v, \hat{A}_{v'}] = [\hat{A}_v, \hat{B}_p] = [\hat{B}_p, \hat{B}_{p'}] = 0$ , making the model exactly solvable. Since  $\hat{B}_p^2 = \hat{A}_v^2 = \mathbf{1}$ , the eigenstates can be labelled by the eigenvalues  $A_v = \pm 1$  and  $B_p = \pm 1$  for each vertex and plaquette. On a torus, where it can be shown that  $\prod_v \hat{A}_v = \prod_p \hat{B}_p = \mathbf{1}$ , the eigenstates are further divided into four superselection sectors, identified by the  $\pm 1$  eigenvalues of two operators  $\hat{O}_x = \prod_{i \in \Lambda_x} \hat{X}_i$  and  $\hat{O}_y = \prod_{i \in \Lambda_y} \hat{X}_i$  spanning the torus along horizontal ( $\Lambda_x$ ) and vertical ( $\Lambda_y$ ) noncontractible circles, respectively, and commuting with all  $\hat{A}_v$  and  $\hat{B}_p$  [Fig. 1(a)]. The model has four ground states, distinguished by the eigenvalues of  $\hat{O}_x$  and  $\hat{O}_y$ , which satisfy  $A_v = B_p = 1$ . Flipping one value  $A_v = -1$  ( $B_p = -1$ ), costs an exci-

tation energy  $g$  and is interpreted as the creation of a quasiparticle, called  $e$  ( $m$ ), on top of the ground state ( $\mathbb{1}_{\text{tc}}$ ), which is localized at the corresponding vertex  $v$  (plaquette  $p$ ). While  $e$  and  $m$  are (hardcore) bosons under self-exchange, they are mutual semions: the wavefunction picks up a  $\pi$  phase when  $m$  is wound around  $e$ , or vice versa. This implies that a bound state  $\psi = e \times m$  of an  $e$  and  $m$  particle, costing an energy  $\mu_\psi = 2g$ , is a fermion, while still being a semion with respect to a separate  $e$  or  $m$ . These quasiparticles, including  $\mathbb{1}_{\text{tc}}$ , represent the four anyon types in the toric code. They are Abelian, since their non-trivial fusion has only one possible outcome:  $e \times m = \psi$ ,  $e \times \psi = m$ ,  $m \times \psi = e$ .

We add to  $\hat{H}_{\text{tc}}$  a local time-periodic drive, whose goal is to induce motion of  $\psi$  fermions and imbue them with a topologically non-trivial band structure. As detailed in the following, non-Abelian character will emerge thanks to the key interplay between the fermion band topology, achieved through Floquet engineering, and the semionic relation between  $\psi$  and  $e$  Abelian anyons, provided by the underlying toric-code model. The drive Hamiltonian is chosen as

$$\hat{H}_d(t) = - \sum_p [d_x(t) \hat{X}_{p,R} \hat{Z}_{p,B} + d_y(t) \hat{X}_{p,T} \hat{Z}_{p,L}], \quad (2)$$

where the subscripts  $(p, j)$ , with  $j \in \{B, R, T, L\}$  denote the spins at the bottom, right, top or left of plaquette  $p$ , respectively [Fig. 1(a)]. Two-body couplings of the form  $\hat{X}_i \hat{Z}_j$  on adjacent spins induce  $\psi$  movement and pairing, as sketched in Fig. 1(a): they consistently displace a joint pair of neighbouring  $e$  and  $m$ , as well as create and annihilate pairs of them. Indeed, since  $\hat{X}_i$  anticommutes with  $\hat{B}_p$  on neighbouring plaquettes  $p$  and  $p'$  and commutes with  $\hat{A}_v$ , its action on an eigenstate flips the corresponding eigenvalues  $B_p$  and  $B_{p'}$ , while preserving the  $e$ -anyon parity  $(-1)^{B_p + B_{p'}}$ . Hence, if a  $m$ -particle composing a fermion is present at  $p$ , it will tunnel to  $p'$  (and vice versa). If no fermion or a pair is present, the associated pair of  $m$  will be created or annihilated, respectively. An equivalent analysis applies to  $e$ -motion on nearby vertices induced by  $\hat{Z}_j$ . The time-periodic control functions  $d_x(t) = d_x(t+T)$  and  $d_y(t) = d_y(t+T)$ , to be specified below, govern processes along the horizontal and vertical direction of the lattice, respectively.

To focus on the behaviour of the  $\psi$  quasiparticles, we adopt the quasiparticle picture of Ref. [21] [details in the Supplemental Material (SM) [22]]. The spins' Hilbert space is mapped to the tensor product of Fock spaces for  $e$  hardcore-boson and  $\psi$  fermion occupations, and of a four-dimensional Hilbert space reflecting four different superselection sectors. In a given sector, the spin operators map to creation and annihilation operators of bosons on vertices ( $\hat{b}_v^\dagger, \hat{b}_v$ ) and of fermions on plaquettes ( $\hat{f}_p^\dagger, \hat{f}_p$ ), with the toric-code ground state  $|0_{\text{tc}}\rangle$  representing the quasiparticle vacuum. The Hamiltonian  $\hat{H}_{\text{tc}}$ , up to constant

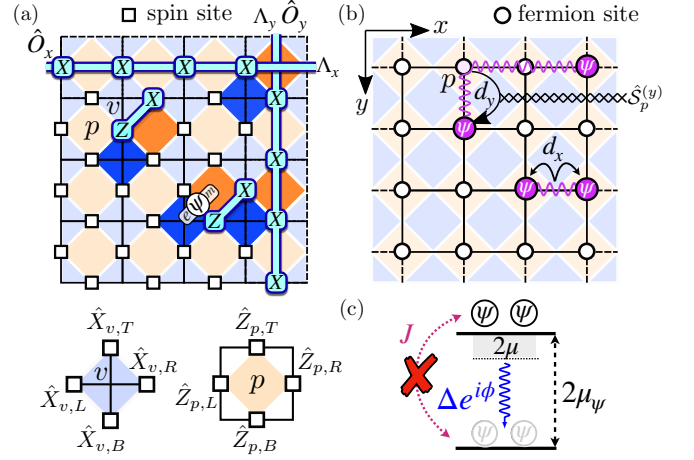


FIG. 1. (a) Spin lattice of the toric code. The  $m$  anyons live on plaquettes  $p$  (orange), while  $e$  anyons live on vertices  $v$  (blue), and their bound state forms a fermion  $\psi$ . The eigenvalues of the operators  $\hat{O}_x$  and  $\hat{O}_y$  define four superselection sectors in the undriven system. The operators  $\hat{X}_i \hat{Z}_j$  depicted induce fermion tunnelling and pairing. Dashed lines indicate periodic boundaries. (b) Lattice for  $\psi$  fermions resulting from the quasiparticle mapping. The drives  $d_x$  and  $d_y$  rule fermion tunnelling and pairing along the horizontal and vertical direction, respectively, with the latter including also a string operators  $\hat{S}_p^{(y)}$  reproducing the semionic statistics of  $\psi$  and  $e$ . (c) Drive-assisted fermion pairing, restoring otherwise off-resonant ( $J \ll \mu_\psi$ ) processes with rate  $\Delta$  and phase  $\phi$ .

energy shifts, maps to  $\hat{H}_e + \hat{H}_{e\psi}^{(0)}$  with the Hamiltonians  $\hat{H}_e = g \sum_v \hat{b}_v^\dagger \hat{b}_v$  and  $\hat{H}_{e\psi}^{(0)} = g \sum_p [1 - \hat{b}_{v(p)}^\dagger \hat{b}_{v(p)}] \hat{f}_p^\dagger \hat{f}_p$ , describing  $e$  and  $\psi$  particles at rest, respectively, where  $v(p)$  denotes the vertex to the bottom-left of  $p$ . The drive  $\hat{H}_d(t)$  maps to a coupling Hamiltonian  $\hat{H}_{e\psi}^{(d)}(t)$ , which describes the driven fermion tunnelling and pairing as well as anyon effects resulting from the fermion motion with respect to the  $e$  bosons. Since  $\hat{H}_d(t)$  drives only the fermions, one can show that  $[\hat{H}_e, \hat{H}_{e\psi}^{(d)}(t)] = 0$  and analyse separately the fermion Hamiltonian  $\hat{H}_\psi(t) = \langle \vec{n}^e | \hat{H}_{e\psi}^{(0)} + \hat{H}_{e\psi}^{(d)}(t) | \vec{n}^e \rangle$  corresponding to a fixed ground state distribution of  $e$  particles on the lattice, encoded in a  $e$ -boson Fock state  $|\vec{n}^e\rangle = (\hat{b}_{v_1}^\dagger)^{n_1} \dots (\hat{b}_{v_N}^\dagger)^{n_N} |0_{\text{tc}}\rangle$ . The presence of  $e$ -bosons at vertices  $\{v\}$  is assumed to derive from preparing the ground state of a toric-code Hamiltonian (1) with inverted coupling  $g \rightarrow \tilde{g} = -g$  for the vertices  $\{v\}$ . Then, the fermion Hamiltonian becomes

$$\begin{aligned} \hat{H}_\psi(t) = & \sum_p [\mu_\psi \hat{f}_p^\dagger \hat{f}_p \\ & - \sum_{r \in \{x, y\}} d_r(t) \mathcal{S}_p^{(r)} (\hat{f}_p \hat{f}_{p+r} + \hat{f}_p^\dagger \hat{f}_{p+r} + \text{H.c.})]. \quad (3) \end{aligned}$$

While  $\mathcal{S}_p^{(x)} = 1$  in Eq. (3), the string  $\mathcal{S}_p^{(y)} = \langle \vec{n}^e | \prod_{v \in \mathbb{R}[v(p)]} (-1)^{\hat{b}_v^\dagger \hat{b}_v} | \vec{n}^e \rangle$  explicitly enforces the

semionic statistics between  $\psi$  and  $e$ . Here,  $R[v(p)]$  denotes all the vertices to the right of the spin shared by the plaquettes  $p$  and  $p + y$  [as in Fig. 1(b)]. Considering a fermion tunnelling on a loop encircling a  $e$  particle,  $\mathcal{S}_p^{(r)}$  indeed reproduces the accumulation of  $\pi$  phase.

*Floquet engineering.* The driven Hamiltonian (3) describes spinless superconducting fermions, with tunnelling and pairing induced by  $\hat{H}_d(t)$ . They are further coupled to a deconfined  $\mathbb{Z}_2$  gauge field given by a background distribution of  $\mathbb{Z}_2$  vortices ( $e$  particles), through  $\hat{\mathcal{S}}_p^{(r)}$ . These ingredients suggest a potential analogy to  $p + ip$  topological superconductors [1, 15, 23], if the bulk fermion bands are gapped and topological. In such systems, fermions can fractionalize into Majorana zero modes localized at the  $\mathbb{Z}_2$  vortices, which then become non-Abelian Ising anyons with non-trivial fusion rules  $e \times e = \mathbb{1}_{\text{is}} + \psi$ ,  $\psi \times \psi = \mathbb{1}_{\text{is}}$ ,  $\psi \times e = e$  [1, 8]. The multiple fusion channels for  $e$ , yielding either the vacuum  $\mathbb{1}_{\text{is}}$  or a fermion  $\psi$ , qualify them as non-Abelian. In the lattice model (3),  $p + ip$  symmetry requires inequivalent pairing terms  $\Delta_r f_p^\dagger f_{p+r}^\dagger$  along  $x$  and  $y$  of the form  $(\Delta_x, \Delta_y) = (\Delta, i\Delta)$  [24]. However, since only control of the underlying toric-code spins is permitted, rather than on the quasiparticle pairing terms directly, no choice of constant  $d_x$  and  $d_y$  can realize the desired  $p + ip$  coupling. Indeed, the functions  $d_r(t)$  need be real-valued and they induce tunnelling and pairing with equal real rate. To overcome these limitations, we employ a periodic time-dependence in  $d_r(t)$  and Floquet engineering [25, 26]. The driving functions are chosen of the form

$$d_r(t) = J + 2\Delta \cos(\omega t + \phi_r). \quad (4)$$

They are time periodic with period  $T = 2\pi/\omega$  and only differ in their driving phase  $\phi_r$ . The amplitudes  $J$  and  $\Delta$  are chosen to be much smaller than the fermion chemical potential,  $J, \Delta \ll \mu_\psi$ . In this weak-driving regime, complex pairing can be achieved effectively as follows. Considering first  $\Delta = 0$ , the energy  $2\mu_\psi$  required for pair creation and annihilation is much larger than  $J$ , and pairing processes are thus far off resonant and effectively suppressed, leaving only quasiparticle tunnelling. They can be restored, however, via the periodic drive, by choosing  $\Delta \neq 0$  and a frequency  $\omega$  matching  $2\mu_\psi$  [Fig. 1(c)]. The advantage is that a complex phase can be attributed to the drive-induced pairing coupling, which depends on the phases  $\phi_r$  of the drives. We thus choose  $\omega = 2(\mu_\psi + \mu)$ , nearly resonant with the fermion-pair energy and allowing for a small detuning  $2\mu$ . Applying Floquet theory [27, 28], the stroboscopic dynamics  $\hat{U}(t_0 + nT)$  generated by the Hamiltonian (3) in steps of  $T$  is ruled by an effective Floquet Hamiltonian  $\hat{H}_F$ , which can be approximated from  $\hat{H}_\psi(t)$  by means of high-frequency expansions, in the regime  $\omega \gg J, \Delta, \mu$  considered here [25, 26, 29–31]. To compute  $\hat{H}_F$  (full derivation in [22]), it is convenient to first shift the

on-site energies by  $\omega/2$  with the gauge transformation  $\hat{R}(t) = \exp[-it(\omega/2) \sum_p \hat{f}_p^\dagger \hat{f}_p]$ . To leading order, the Floquet Hamiltonian in this frame is given by the time average  $\hat{H}_F = \frac{1}{T} \int_0^T dt \hat{H}'_\psi(t)$  of the transformed Hamiltonian  $\hat{H}'_\psi(t) = \hat{R}^\dagger(t) \hat{H}_\psi(t) \hat{R}(t) - i\hat{R}^\dagger(t) \partial_t \hat{R}(t)$ , which is still  $\omega$ -periodic, and reads

$$\begin{aligned} \hat{H}_F = & -\mu \sum_p \hat{f}_p^\dagger \hat{f}_p \\ & - \sum_{r=x,y} \mathcal{S}_p^{(r)} (\Delta e^{i\phi_r} \hat{f}_p \hat{f}_{p+r} + J \hat{f}_p^\dagger \hat{f}_{p+r} + \text{H.c.}) . \end{aligned} \quad (5)$$

The stroboscopic propagator reads  $\hat{U}(T) = \hat{R}(T) e^{-i\hat{H}_F T}$ . At time  $T$ , the transformation  $\hat{R}(t)$  reduces to the total fermion parity of the system,  $\hat{R}(T) = \exp(-i\pi \sum_p \hat{f}_p^\dagger \hat{f}_p) = (-1)^{\sum_p \hat{f}_p^\dagger \hat{f}_p}$ , which is a conserved quantity in the driven (and thus also the Floquet) Hamiltonian. Since quasiparticles in the toric code can only be created in pairs, only even-parity states are physical and, given that  $R(T) = 1$  in their subspace, their stroboscopic dynamics is ruled by  $\hat{H}_F$  of Eq. (5).

From Eq. (5), we obtain pairing with  $p + ip$  symmetry by choosing a circular-like shaking, with phase delay  $\phi_y - \phi_x = \pi/2$  between horizontal and vertical drives. The high-frequency effective Hamiltonian, Eq. (5), then describes spinless superconducting  $\psi$  fermions with  $p + ip$  pairing, a chemical potential  $\mu$  controlled by the detuning of the drive from the fermion-pair chemical potential of the toric code and coupled to the  $\mathbb{Z}_2$  vortices via  $\hat{\mathcal{S}}_p^{(r)}$ . We next verify that the driven model hosts Floquet-Majorana modes and realizes Ising anyons.

*Floquet-Majorana modes.* For weak driving, the fermions reproduce faithfully the behaviour of a topological superconductor, as described by the time-averaged Hamiltonian (5). We study these properties by numerically computing the exact Floquet Bogoliubov-de Gennes (FBdG) Hamiltonian  $\hat{H}_{\text{FBdG}}$ , defined by  $\hat{H}_F = (1/2)(\hat{\mathbf{f}}^\dagger, \hat{\mathbf{f}}) \hat{H}_{\text{FBdG}} (\hat{\mathbf{f}}, \hat{\mathbf{f}}^\dagger)^T$ , as well as its quasienergy spectrum and ground state parity, from the driven Hamiltonian of Eq. (3) [22]. This is done through the diagonalization of the one-cycle evolution operator  $\hat{U}(T)$  and of the quasienergy operator in Floquet space [30]. In the absence of vortices [ $\mathcal{S}_p^{(r)} = 1$ ], we find four nearly-degenerate Floquet high-frequency ‘ground’ states, one in each superselection sector corresponding to periodic or anti-periodic boundary conditions for the fermions in each direction [15], as given by the absence or presence of a  $e$  particle in the holes of the torus. The topological phase, characterized by a non-zero Chern number of the negative-energy fermion band, is expected for  $|\mu| < 4J$  [15, 24, 32]. In such a phase, only three ground states have even fermion parity and are thus physical, corresponding to the three Ising-anyon types  $e, 1, \psi$ . Choosing the driving frequency  $\omega$  such that the effective chemical potential is in the topological region,  $\mu \simeq -2J$ ,

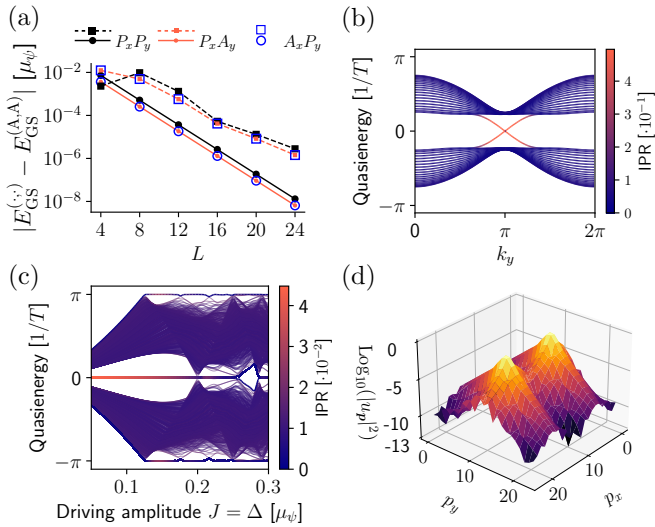


FIG. 2. (a) Splitting between fermion ground states for  $\mu = -2J$  in different superselection sectors, characterized by periodic ( $P_{x/y}$ ) or anti-periodic ( $A_{x/y}$ ) boundary conditions and having energy  $E_{GS}^{(x,y)}$  [ $(x,y)$  denotes the boundary condition]. The  $P_x P_y$  ground state has odd parity. Solid lines and circles denote results in the high-frequency regime ( $J = \Delta = 0.1\mu_\psi$ ), while dashed lines and squares correspond to the anomalous phase ( $J = \Delta = 0.15\mu_\psi$ ) (b) FBdG quasienergy spectrum and edge modes on a  $L_x \times L_y = 20 \times 200$  cylinder, periodic along  $x$ , for  $J = \Delta = 0.1\mu_\psi$ . The color scale indicates the inverse participation ratio of the corresponding FBdG eigenstate. (c) FBdG quasienergy spectrum for  $\mu = -2J$  and  $L = 24$  for increasing  $J = \Delta$ . (d) Coefficients  $\log_{10} |u_p^T|^2$  of the zero mode defined by  $\hat{\alpha}_1^\dagger = \sum_p (v_p \hat{f}_p + u_p^T \hat{f}_p^\dagger)$  with  $v_p \simeq u_p^*$ , for  $J = \Delta = 0.1\mu_\psi$  and  $L = 24$ .

the fourfold degeneracy is approached exponentially as the system size increases, as shown in Fig. (2)(a), and agrees with the predicted fermion parities. On a cylinder, the quasienergy spectrum exhibits two edge modes [Fig. 1(b)], signalling the achievement of non-zero Chern number, which disappears for  $|\mu| > 4J$ .

When introducing two vortices at separate positions on the torus, approximate Majorana modes at near-zero quasienergy appear: they persist as  $\omega$  is detuned from resonance within the topological phase and are exponentially localized around the vortices [Fig. 2(d)]. This confirms that the high-frequency description of Eq. (5) correctly captures the topological properties of the system, which are not spoiled by the higher-order contributions to the high-frequency expansion neglected in (5). Those terms, besides renormalizing the couplings in  $\hat{H}_F$ , generically contain coupling terms of progressively longer range [30, 33]. Increasing the driving amplitudes  $J = \Delta$ , while keeping  $\mu = -2J$  to stay in the topological phase, the driven fermions enter an anomalous Floquet-topological phase [26, 34, 35] as they depart from the high-frequency limit. Although, in this regime, the description in terms of the time-averaged Hamiltonian of

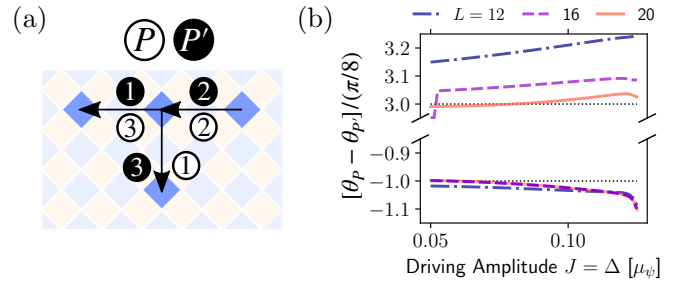


FIG. 3. (a) Paths  $P$  and  $P'$  involved in the vortex-exchange protocol. The phase difference between the two cases determines the exchange phase. (b) Vortex exchange phase  $\theta_P - \theta_{P'}$  for  $\omega = 2(\mu_\psi - 2J)$ , different system size and driving amplitude in the high-frequency regime. The upper (lower) panel shows the phase for doubly-periodic (anti-periodic) fermion boundary conditions, corresponding to the  $\psi$  ( $\mathbb{1}_{is}$ ) sector.

Eq. (5) is no longer valid, the system still exhibits Majorana modes, at both quasienergy zero and  $\pm\pi/T$ , see Fig. 2(c). This effect is only possible in driven systems [34, 36–38] and, in the context of Kitaev quantum wires, has been proposed as a means to realize non-Abelian braiding and quantum computation with edge modes in 1D [39–42].

*Non-Abelian exchange phases.* We next analyze the exchange statistics of  $e$  vortices in the fermion topological phase, to verify whether they realize non-Abelian statistics as predicted in the presence of Majorana modes [8, 23]. In the weak-driving regime, the ground state of the time-averaged effective Hamiltonian may be prepared adiabatically from the ground state of the undriven model by slowly ramping up the Floquet modulation [43, 44], which also averages out micromotion effects related to the global phase of the drives [29]. We exchange a pair of vortices using the approach of Ref. [21], based on Levin-Wen’s protocol [8, 45, 46] and sketched in Fig. 3(a). Such a protocol compares the phase accumulated by moving the vortices along two paths  $P$  and  $P'$  sharing the same set of vortex positions, but where the vortices are moved in different order. This guarantees that the Berry-phase difference between the two paths is determined by the exchange statistics only. With the allowed control on the toric-code spins, the operators moving a vortex between nearby vertices  $v$  and  $v+r$  are the Pauli operators  $\hat{Z}_{v,R}$  (for  $r=x$ ) and  $\hat{Z}_{v,B}$  (for  $r=y$ ) acting on the spin shared between them. In the quasiparticle picture, the latter map to quasiparticle operators  $\hat{t}_v^{(r)} = \hat{\mathcal{S}}_v^{(r)} (\hat{b}_v^\dagger + \hat{b}_v) (\hat{b}_{v+r}^\dagger + \hat{b}_{v+r})$ , inducing boson motion and also containing a fermionic part to account for semionic statistics,  $\hat{\mathcal{S}}_v^{(x)} = 1$  and  $\hat{\mathcal{S}}_v^{(y)} = \prod_{p \in L[p(v+y)]} (-1)^{\hat{f}_p^\dagger \hat{f}_p}$ , where  $L[p(v+y)]$  denotes all plaquettes to the left of the spin shared by  $v$  and  $v+y$ . A vortex may be moved by locally realizing the single-spin transformation  $\hat{Z}_{v,\alpha}$  through a Floquet-

adiabatic process. For each intermediate vortex configuration  $|\vec{n}_i^e\rangle$  along the exchange paths, the fermions realize the corresponding BCS even-parity ground state  $|\Phi_i\rangle$  of the FBdG Hamiltonian, which we determine numerically. The Berry phase accumulated along the path  $P$  is computed as  $\theta_P = \text{Arg} \prod_{(i,i+1) \in P} \langle \Phi_{i+1} | \hat{S}_{i+1,i}^{(r)} | \Phi_i \rangle$ , where we indicated with  $\hat{S}_{i+1,i}^{(r)}$  the fermionic part of the vortex-displacement operator  $\hat{t}_v^{(r)}$  which converts the vortex configuration  $|\vec{n}_i^e\rangle$  into  $|\vec{n}_{i+1}^e\rangle$  by moving one vortex. Details about the numerical evaluation of the matrix elements are given in the SM [22]. Exchange in the different vortex fusion sectors  $\mathbb{1}_{\text{is}}$  and  $\psi$  can be distinguished by computing the exchange phase with doubly-anti-periodic and doubly-periodic fermion boundary conditions, respectively [21]. Indeed, in the anti-periodic case, the even-parity ground state is the quasiparticle vacuum, such that the pair of vortices is created and annihilates in the  $\mathbb{1}_{\text{is}}$  sector. For the periodic case, the FBdG ground state has odd parity and thus the physical even-parity ground state is the first-excited state containing one FBdG fermionic quasiparticle. The vortex pair thus fuses to a fermion. The counterclockwise exchange phases obtained are shown in Fig 3(b), for varying driving amplitude and for different system size. The results converge rapidly with the size towards the prediction for Ising topological order,  $R_{\mathbb{1}_{\text{is}}}^{ee} = e^{-i\pi C/8}$  and  $R_{\psi}^{ee} = e^{3i\pi C/8}$  for fermion Chern number  $C = 1$ . The  $\pi/2$  difference between the exchange phase in the two different sectors supports non-Abelian behaviour [47]. Inverting the sign of the driving phase-shift,  $\phi_y - \phi_x = -\pi/2$ , hence inverting the handedness of the circular drive, inverts the sign of the exchange phases. We have thus shown that the zero modes developed by the driven toric code in the high-frequency regime behave as Ising anyons.

*Conclusion.* With the example of the toric-code model, we have shown that time-periodic driving of an Abelian-anyon system can lead to the emergence of non-Abelian topological order. The ideas presented here may be extended to other 2D topologically ordered systems, building on the property that anyon quasiparticles, being spatially localized, can generically be driven by means of local control, as proposed here. Moreover, they indicate a potential path towards non-Abelian physics, by exploiting out-of-equilibrium Abelian phases as recently realized in engineered quantum systems [5–7].

The author is grateful to André Eckardt, Nathan Harshman, Alexander Schnell and Isaac Tesfaye for helpful and inspiring discussions.

---

[1] C. Nayak, S. H. Simon, A. Stern, M. Freedman, and S. Das Sarma, Non-Abelian anyons and topological quantum computation, *Rev. Mod. Phys.* **80**, 1083 (2008).

- [2] L. Savary and L. Balents, Quantum spin liquids: a review, *Rep. Progr. Phys.* **80**, 016502 (2016).
- [3] A. Kitaev, Fault-tolerant quantum computation by anyons, *Ann. Phys.* **303**, 2 (2003).
- [4] H.-N. Dai, B. Yang, A. Reingruber, H. Sun, X.-F. Xu, Y.-A. Chen, Z.-S. Yuan, and J.-W. Pan, Four-body ring-exchange interactions and anyonic statistics within a minimal toric-code Hamiltonian, *Nat. Phys.* **13**, 1195 (2017).
- [5] J. Kwan, P. Segura, Y. Li, S. Kim, A. V. Gorshkov, A. Eckardt, B. Bakkali-Hassani, and M. Greiner, Realization of 1D Anyons with Arbitrary Statistical Phase (2023), arXiv:2306.01737 [cond-mat.quant-gas].
- [6] G. Semeghini, H. Levine, A. Keesling, S. Ebadi, T. T. Wang, D. Bluvstein, R. Verresen, H. Pichler, M. Kalinowski, R. Samajdar, A. Omran, S. Sachdev, A. Vishwanath, M. Greiner, V. Vuletić, and M. D. Lukin, Probing topological spin liquids on a programmable quantum simulator, *Science* **374**, 1242 (2021).
- [7] K. J. Satzinger, Y.-J. Liu, A. Smith, C. Knapp, M. Newman, C. Jones, Z. Chen, C. Quintana, X. Mi, A. Dunsworth, C. Gidney, I. Aleiner, F. Arute, K. Arya, J. Atalaya, and et al., Realizing topologically ordered states on a quantum processor, *Science* **374**, 1237 (2021).
- [8] A. Kitaev and J. Preskill, Topological Entanglement Entropy, *Phys. Rev. Lett.* **96**, 110404 (2006).
- [9] H. Bombin, Topological Order with a Twist: Ising Anyons from an Abelian Model, *Phys. Rev. Lett.* **105**, 030403 (2010).
- [10] J. R. Wootton, V. Lahtinen, Z. Wang, and J. K. Pachos, Non-Abelian statistics from an Abelian model, *Phys. Rev. B* **78**, 161102 (2008).
- [11] G. Q. AI and collaborators, Non-Abelian braiding of graph vertices in a superconducting processor, *Nature* **618**, 264 (2023).
- [12] H. C. Po, L. Fidkowski, T. Morimoto, A. C. Potter, and A. Vishwanath, Chiral Floquet Phases of Many-Body Localized Bosons, *Phys. Rev. X* **6**, 041070 (2016).
- [13] H. C. Po, L. Fidkowski, A. Vishwanath, and A. C. Potter, Radical chiral Floquet phases in a periodically driven Kitaev model and beyond, *Phys. Rev. B* **96**, 245116 (2017).
- [14] H.-K. Jin, J. Knolle, and M. Knap, Fractionalized Prethermalization in a Driven Quantum Spin Liquid, *Phys. Rev. Lett.* **130**, 226701 (2023).
- [15] N. Read and D. Green, Paired states of fermions in two dimensions with breaking of parity and time-reversal symmetries and the fractional quantum Hall effect, *Phys. Rev. B* **61**, 10267 (2000).
- [16] G. Moore and N. Read, Nonabelions in the fractional quantum Hall effect, *Nuclear Physics B* **360**, 362 (1991).
- [17] H. Weimer, M. Müller, I. Lesanovsky, P. Zoller, and H. P. Büchler, A Rydberg quantum simulator, *Nat. Phys.* **6**, 382 (2010).
- [18] M. Sameti, A. Potočnik, D. E. Browne, A. Wallraff, and M. J. Hartmann, Superconducting quantum simulator for topological order and the toric code, *Phys. Rev. A* **95**, 042330 (2017).
- [19] F. Petiziol, S. Wimberger, A. Eckardt, and F. Mintert, Non-perturbative Floquet engineering of the toric-code Hamiltonian and its ground state (2023), arXiv:2211.09724 [quant-ph].
- [20] X.-G. Wen, Quantum Orders in an Exact Soluble Model, *Phys. Rev. Lett.* **90**, 016803 (2003).
- [21] C. Chen, P. Rao, and I. Sodemann, Berry phases of vison

- transport in  $\mathbb{Z}_2$  topologically ordered states from exact fermion-flux lattice dualities, *Phys. Rev. Res.* **4**, 043003 (2022).
- [22] see the Supplemental Material, where we discuss (i) the quasiparticle mapping to how the inequalities for the control variables are solved; (ii) details about the high-frequency expansion yielding the effective Floquet Hamiltonian of Eq. (5); (iii) details about the computation of the BCS-like ground states of the Floquet Bogoliubov-de Gennes Hamiltonian and of the vortex exchange phases..
- [23] D. A. Ivanov, Non-Abelian Statistics of Half-Quantum Vortices in  $p$ -Wave Superconductors, *Phys. Rev. Lett.* **86**, 268 (2001).
- [24] S. Sachdev, *Quantum Phases of Matter* (Cambridge University Press, 2023).
- [25] M. Bukov, L. D'Alessio, and A. Polkovnikov, Universal high-frequency behavior of periodically driven systems: from dynamical stabilization to Floquet engineering, *Adv. Phys.* **64**, 139 (2015).
- [26] A. Eckardt, Colloquium: Atomic quantum gases in periodically driven optical lattices, *Rev. Mod. Phys.* **89**, 011004 (2017).
- [27] J. H. Shirley, Solution of the Schrödinger Equation with a Hamiltonian Periodic in Time, *Phys. Rev.* **138**, B979 (1965).
- [28] H. Samba, Steady States and Quasienergies of a Quantum-Mechanical System in an Oscillating Field, *Phys. Rev. A* **7**, 2203 (1973).
- [29] N. Goldman and J. Dalibard, Periodically Driven Quantum Systems: Effective Hamiltonians and Engineered Gauge Fields, *Phys. Rev. X* **4**, 031027 (2014).
- [30] A. Eckardt and E. Anisimovas, High-frequency approximation for periodically driven quantum systems from a Floquet-space perspective, *New J. Phys.* **17**, 093039 (2015).
- [31] T. Mikami, S. Kitamura, K. Yasuda, N. Tsuji, T. Oka, and H. Aoki, Brillouin-Wigner theory for high-frequency expansion in periodically driven systems: Application to Floquet topological insulators, *Phys. Rev. B* **93**, 144307 (2016).
- [32] M. Sato and Y. Ando, Topological superconductors: a review, *Reports on Progress in Physics* **80**, 076501 (2017).
- [33] F. Petiziol, M. Sameti, S. Carretta, S. Wimberger, and F. Mintert, Quantum Simulation of Three-Body Interactions in Weakly Driven Quantum Systems, *Phys. Rev. Lett.* **126**, 250504 (2021).
- [34] L. Jiang, T. Kitagawa, J. Alicea, A. R. Akhmerov, D. Pekker, G. Refael, J. I. Cirac, E. Demler, M. D. Lukin, and P. Zoller, Majorana Fermions in Equilibrium and in Driven Cold-Atom Quantum Wires, *Phys. Rev. Lett.* **106**, 220402 (2011).
- [35] M. S. Rudner, N. H. Lindner, E. Berg, and M. Levin, Anomalous Edge States and the Bulk-Edge Correspondence for Periodically Driven Two-Dimensional Systems, *Phys. Rev. X* **3**, 031005 (2013).
- [36] D. E. Liu, A. Levchenko, and H. U. Baranger, Floquet Majorana Fermions for Topological Qubits in Superconducting Devices and Cold-Atom Systems, *Phys. Rev. Lett.* **111**, 047002 (2013).
- [37] Q.-J. Tong, J.-H. An, J. Gong, H.-G. Luo, and C. H. Oh, Generating many Majorana modes via periodic driving: A superconductor model, *Phys. Rev. B* **87**, 201109 (2013).
- [38] J. K. Asbóth, B. Tarasinski, and P. Delplace, Chiral symmetry and bulk-boundary correspondence in periodically driven one-dimensional systems, *Phys. Rev. B* **90**, 125143 (2014).
- [39] R. W. Bomantara and J. Gong, Simulation of Non-Abelian Braiding in Majorana Time Crystals, *Phys. Rev. Lett.* **120**, 230405 (2018).
- [40] R. W. Bomantara and J. Gong, Quantum computation via Floquet topological edge modes, *Phys. Rev. B* **98**, 165421 (2018).
- [41] B. Bauer, T. Pereg-Barnea, T. Karzig, M.-T. Rieder, G. Refael, E. Berg, and Y. Oreg, Topologically protected braiding in a single wire using Floquet Majorana modes, *Phys. Rev. B* **100**, 041102 (2019).
- [42] R. W. Bomantara and J. Gong, Measurement-only quantum computation with Floquet Majorana corner modes, *Phys. Rev. B* **101**, 085401 (2020).
- [43] H. Breuer and M. Holthaus, Quantum phases and Landau-Zener transitions in oscillating fields, *Physics Letters A* **140**, 507 (1989).
- [44] A. Eckardt and M. Holthaus, Avoided-Level-Crossing Spectroscopy with Dressed Matter Waves, *Phys. Rev. Lett.* **101**, 245302 (2008).
- [45] M. Levin and X.-G. Wen, Fermions, strings, and gauge fields in lattice spin models, *Phys. Rev. B* **67**, 245316 (2003).
- [46] K. Kawagoe and M. Levin, Microscopic definitions of anyon data, *Phys. Rev. B* **101**, 115113 (2020).
- [47] M. Cheng, V. Galitski, and S. Das Sarma, Nonadiabatic effects in the braiding of non-Abelian anyons in topological superconductors, *Phys. Rev. B* **84**, 104529 (2011).
- [48] P. Ring and P. Schuck, *The Nuclear Many-Body Problem* (Springer-Verlag Berlin Heidelberg, Oxford, 1980).
- [49] L. M. Robledo, Sign of the overlap of Hartree-Fock-Bogoliubov wave functions, *Physical Review C - Nuclear Physics* **79**, 1 (2009).

# Supplemental Material to Non-Abelian anyons in a periodically-driven Abelian model

Francesco Petziol

*Technische Universität Berlin, Institut für Theoretische Physik, Hardenbergstraße 36, Berlin 10623, Germany*

## QUASIPARTICLE MAPPING

We review in this section the quasiparticle mapping of Ref. [21] and apply it to the driven toric-code model of Eq. (1) and (2) on a torus.

We use the notation  $p(v)$  to indicate the plaquette situated to the immediate top-right of a vertex  $v$ , and, conversely,  $v(p)$  to denote the vertex to the bottom-left of the plaquette  $p$ . The set of commuting plaquette and vertex operators  $\hat{B}_p$  and  $\hat{A}_v$  of the toric code, whose  $\pm 1$  eigenvalues are associated with the presence or the absence of  $e$  and  $m$  quasiparticles, represents a complete set of observables on the system Hilbert space on a infinite lattice and an undercomplete one on the torus (since they are not all linearly independent, due to  $\prod_p \hat{B}_p = \prod_v \hat{A}_v = \mathbb{1}$ ). An equivalent commuting set, sharing the same common eigenstates as  $\hat{A}_v$  and  $\hat{B}_p$ , is given by the operators  $\hat{A}_v \hat{B}_{p(v)}$  and  $\hat{B}_p$ , whose  $\pm 1$  eigenvalues can be associated with the presence of  $\psi$  and  $e$  quasiparticles instead. A fermion  $\psi$  is then conventionally interpreted as located on the plaquette  $p$  and composed of a pair of  $m$  and  $e$  anyons occupying the plaquette  $p$  and vertex  $v(p)$ , respectively (as depicted in Fig. 1). The presence (absence) of a fermion is detected by the  $-1$  ( $+1$ ) eigenvalue of  $\hat{B}_p$ , thus counting the parity  $(-1)^{n_p^\psi}$  of the number  $n_p^\psi \in \{0, 1\}$  of fermions potentially occupying the plaquette  $p$ . Similarly, the presence (absence) of an isolated  $e$  boson is detected by the  $-1$  ( $+1$ ) eigenvalue of  $\hat{A}_v \hat{B}_{p(v)}$ . We thus refer to  $\hat{B}_p$  as fermion parity operators and to  $\hat{A}_v \hat{B}_{p(v)}$  as boson parity operators.

The first step of the quasiparticle mapping is to map the toric-code spins to a dual pseudospin space, such that the commuting operators  $\hat{A}_v \hat{B}_{p(v)}$  and  $\hat{B}_p$  with  $\pm 1$  eigenvalues are mapped to commuting pseudospin Pauli- $\hat{Z}$  operators  $\hat{Z}_v^e$  and  $\hat{Z}_p^\psi$  living on the corresponding vertex and plaquette. The dual pseudospin space is the tensor product  $\mathbb{H}_e \otimes \mathbb{H}_\psi$  of a spin-1/2 space  $\mathbb{H}_e$  for boson parities and of a spin-1/2 space  $\mathbb{H}_\psi$  for fermion parities. The pseudospin mapping starts with

$$\hat{Z}_v^e = \hat{A}_v \hat{B}_{p(v)}, \quad \hat{Z}_p^\psi = \hat{B}_p. \quad (\text{S6})$$

On the torus, given the additional constraint that the total  $\psi$  and  $e$  parities are conserved,

$$\prod_v \hat{A}_v \hat{B}_{p(v)} = \mathbb{1}, \quad \prod_p \hat{B}_p = \mathbb{1}, \quad (\text{S7})$$

the local parities do not form a complete set. A complete set is obtained by introducing Wilson-loop opera-

tors which commute with all local parities, such as

$$\hat{W}_x = - \prod_{p \in \tilde{\Gamma}_x} \hat{X}_{p,L} \hat{Z}_{p,T}, \quad \hat{W}_y = - \prod_{p \in \tilde{\Gamma}_y} \hat{X}_{p,B} \hat{Z}_{p,R}, \quad (\text{S8})$$

where the paths  $\tilde{\Gamma}_r$ , with  $r = x, y$ , are depicted in Fig. S1 [when convenient, we use the notation for spin operators defined after Eq. (2) and in Fig. 1(a)]. The Wilson-loop operators describe  $\psi$ -fermion tunnelling all across the torus in horizontal and vertical direction. Their eigenvalues  $\pm 1$  distinguish four superselection sectors and, at the end of the mapping, will correspond to the choice of either periodic ( $W_x = 1$  or  $W_y = 1$ ) or anti-periodic ( $W_x = -1$  or  $W_y = -1$ ) boundary conditions for the fermions. The operators  $\hat{W}_x$  are mapped to two pseudospins  $\hat{Z}_r^W$  in the two-spin space  $\mathbb{H}_W$ , such that the total pseudospin Hilbert space on the torus has the structure  $\mathbb{H}_e \otimes \mathbb{H}_\psi \otimes \mathbb{H}_W$ . Due to the total fermion and boson parity conservation, single-pseudospin Pauli- $\hat{X}$ -type operators which anti-commute with a single  $\hat{Z}_v^e$  or  $\hat{Z}_p^\psi$  are not physical and cannot be defined: physical operators may only create and annihilate anyon pairs (in an open-boundary system, they can be defined instead by creating a pair with one anyon at the edge [21]). Instead, one can define two-body pseudospin operators, where one of the two pseudospins is conventionally chosen to be located on the first vertex or plaquette on the top-left of the lattice (Fig. S1). These can be defined, for instance, as

$$\hat{X}_1^e \hat{X}_v^e = \prod_{i \in \Gamma_{1,v}} \hat{Z}_i, \quad (\text{S9a})$$

$$\hat{X}_1^\psi \hat{X}_p^\psi = \prod_{i \in \Gamma_{1,v}} \hat{Z}_i \prod_{j \in \tilde{\Gamma}_{1,p}} \hat{X}_j, \quad (\text{S9b})$$

where  $\Gamma_{1,v}$  is a path connecting vertices 1 and  $v$ , while  $\tilde{\Gamma}_{1,p}$  connects the 1st and the  $p$ th plaquette, with the specific path convention depicted in Fig. S1:  $\Gamma_{1,v}$  descends vertically from the top-left vertex until the vertex row to which  $v$  belongs and the continues horizontally until  $v$ ;  $\tilde{\Gamma}_{1,p}$  connects the top-left plaquette to the right-most one in the same row, descends vertically until the plaquette row to which  $p$  belongs, and then horizontally to reach  $p$ . With this choice, it can be verified that spin anti-commutation rules are satisfied by the pseudospins,  $\{\hat{X}_1^e \hat{X}_v^e, \hat{Z}_v^e\} = 0$  and  $\{\hat{X}_1^\psi \hat{X}_p^\psi, \hat{Z}_p^\psi\} = 0$ .

Using Eqs. (S6) and (S9), the two-spin driving terms of the form  $\hat{X}_i \hat{Z}_j$  entering the drive Hamiltonian  $\hat{H}_d(t)$  of Eq. (2) are mapped to pseudospin operators. The precise mapping depends on whether a term involves spins

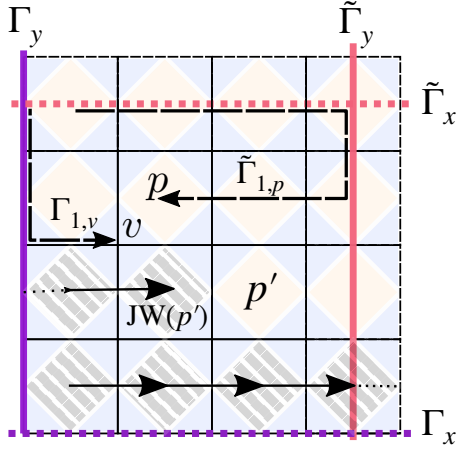


FIG. S1. Paths used in the quasiparticle mapping of Ref. [21] for the pseudospin mapping ( $\Gamma_{x/y}$ ,  $\tilde{\Gamma}_{x/y}$ ,  $\Gamma_{1,v}$  and  $\tilde{\Gamma}_{1,p}$ ) and in the Jordan-Wigner (JW) mapping to fermions.

located on the boundaries, which are intersected by  $\Gamma_r$  or  $\tilde{\Gamma}_r$ , or not [21]. We report, as an example, only the mapping for terms in the bulk, not intersecting the boundary, which reads

$$\hat{X}_{p,R} \hat{Z}_{p,B} = \hat{\mathbf{X}}_p^\psi \hat{\mathbf{X}}_{p+x}^\psi \quad (\text{S10a})$$

$$\hat{X}_{p,L} \hat{Z}_{p,T} = \left( \prod_{v \in \text{R}[v(p)]} \hat{Z}_v^e \right) \left( \prod_{\substack{p' \in \text{L}(p+y) \\ p' \in \text{R}(p)}} \hat{Z}_{p'}^\psi \right) \hat{\mathbf{X}}_p^\psi \hat{\mathbf{X}}_{p+y}^\psi, \quad (\text{S10b})$$

where  $\text{R}(v)$  and  $\text{L}(v)$  denote all vertices to the right and to the left of  $v$ , respectively, and similarly for plaquettes.

After the intermediate pseudospin mapping, the quasiparticle mapping is completed by mapping  $e$  pseudospins to hardcore bosons and  $\psi$  pseudospins to fermions. Specifically, pseudospins of  $e$  type are mapped to hardcore bosons via

$$\hat{Z}_v^e = (-1)^{\hat{b}_v^\dagger \hat{b}_v}, \quad \hat{\mathbf{X}}_v^e = \hat{b}_v^\dagger + \hat{b}_v, \quad (\text{S11})$$

where  $\hat{b}_v^\dagger$  and  $\hat{b}_v$  are bosonic creation and annihilation operators. Equivalently,  $\hat{Z}_v^e = 1 - 2\hat{b}_v^\dagger \hat{b}_v$ , given the hard-core constraint. Pseudospins of  $\psi$  type are mapped, instead, to fermions via a Jordan-Wigner transformation,

$$\hat{Z}_p^\psi = -i\hat{\gamma}_p \hat{\gamma}'_p, \quad \hat{\mathbf{X}}_p^\psi = \left( \prod_{p' \in \text{JW}(p)} \hat{Z}_{p'}^\psi \right) \hat{\gamma}'_p, \quad (\text{S12})$$

where  $\text{JW}(p)$  is a Jordan-Wigner string with the convention shown in Fig. S1: the summation involves all plaquettes scanned left-to-right, row-by-row from the bottom of the lattice up, until  $p$ , thus following the path  $\text{JW}(p)$  depicted in S1. In Eq. (S12), we have introduced

the Majorana real-fermion operators

$$\hat{\gamma}_p = \hat{f}_p + \hat{f}_p^\dagger, \quad \hat{\gamma}'_p = -i(\hat{f}_p - \hat{f}_p^\dagger), \quad (\text{S13})$$

where  $\hat{f}_p^\dagger$  and  $\hat{f}_p$  are creation and annihilation operators for a complex fermion ( $\psi$ ). The two-spin terms of Eq. (S10b) then become

$$\hat{X}_{p,R} \hat{Z}_{p,B} = i\hat{\gamma}_p \hat{\gamma}'_{p+x} \quad (\text{S14a})$$

$$\hat{X}_{p,L} \hat{Z}_{p,T} = \left[ \prod_{v \in \text{R}[v(p)]} (-1)^{\hat{b}_v^\dagger \hat{b}_v} \right] i\hat{\gamma}_p \hat{\gamma}'_{p+y}. \quad (\text{S14b})$$

For two-spin terms inducing fermion motion across the boundaries horizontally and vertically, respectively, the mapping yields

$$\hat{X}_{p,R} \hat{Z}_{p,B} = \left( \prod_{v \in \text{Ab}(p)} (-1)^{\hat{b}_v^\dagger \hat{b}_v} \right) i\hat{\gamma}_p \hat{\gamma}'_{p+x} \hat{\mathbf{Z}}_x^W, \quad (\text{S15a})$$

$$\hat{X}_{p,L} \hat{Z}_{p,T} = \left( \prod_{v \in \text{R}[v(p)]} (-1)^{\hat{b}_v^\dagger \hat{b}_v} \right) i\hat{\gamma}_p \hat{\gamma}'_{p+y} \hat{\mathbf{Z}}_y^W, \quad (\text{S15b})$$

involving the ‘Wilson-loop pseudospins’  $\hat{\mathbf{Z}}_r^W$ , and where  $\text{Ab}(p)$  indicates all vertices above the row of plaquettes to which  $p$  belongs. In the absence of terms in the Hamiltonian that can induce a change of superselection sector (through tunnelling of a  $e$ -boson all around the torus), the choice of sector determined by the eigenvalues of the Wilson loop operators  $\hat{W}_x$  and  $\hat{W}_y$  then implies the choice of either periodic ( $\mathbf{Z}_x^W = +1$ ,  $\mathbf{Z}_y^W = +1$ ) or anti-periodic ( $\mathbf{Z}_x^W = -1$ ,  $\mathbf{Z}_y^W = -1$ ) boundary condition for the fermions along each direction. Defining the string of boson parities

$$\hat{\mathcal{S}}_p^{(y)} = \left[ \prod_{v \in \text{R}[v(p)]} (-1)^{\hat{b}_v^\dagger \hat{b}_v} \right], \quad (\text{S16})$$

the driven toric-code Hamiltonian  $\hat{H}_{\text{tc}} + \hat{H}_d(t)$ , with  $\hat{H}_{\text{tc}}$  of Eq. (1) and  $\hat{H}_d(t)$  of Eq. (2), is then mapped, in the bulk, to

$$\hat{H}(t) = -\frac{g}{2} \sum_v (-1)^{\hat{b}_v^\dagger \hat{b}_v} \quad (\text{S17})$$

$$+ \sum_p \left\{ \frac{g}{2} \left[ 1 + (-1)^{\hat{b}_{v(p)}^\dagger \hat{b}_{v(p)}} \right] i\hat{\gamma}_p \hat{\gamma}'_p + f_x(t) i\hat{\gamma}_p \hat{\gamma}'_{p+x} + f_y(t) \hat{\mathcal{S}}_p^{(y)} i\hat{\gamma}_p \hat{\gamma}'_{p+y} \right\} \quad (\text{S18})$$

Eq. (S22) applies to bulk fermions: We did not explicitly include the corrections for the boundary terms, which we dump on the choice of boundary condition (we also assume that  $e$  bosons are present only in the bulk). We next make the assumption that, whenever an  $e$ -boson pair is present at vertices  $v$  and  $v'$ , such that  $\hat{b}_v^\dagger \hat{b}_v =$

$\hat{b}_v^\dagger, \hat{b}_{v'} = 1$ , this corresponds to using a slightly modified toric-code Hamiltonian in Eq. (1) with  $g\hat{A}_v \rightarrow -g\hat{A}_v$  and  $g\hat{A}_{v'} \rightarrow -g\hat{A}_{v'}$ , namely

$$\hat{H}_{\text{tc}} = \frac{g}{2}(\hat{A}_v + \hat{A}_{v'}) - \frac{g}{2} \sum_{v'' \neq v, v'} \hat{A}_{v''} - \frac{g}{2} \sum_p \hat{B}_p, \quad (\text{S19})$$

such that the state containing the  $e$  pair is the ground state with respect to the modified Hamiltonian. In this case, the Hamiltonian (S22), for a fixed configuration of  $e$  bosons defined by a boson Fock state  $|\vec{n}^e\rangle = (\hat{b}_{v_1}^\dagger)^{n_1} \dots (\hat{b}_{v_N}^\dagger)^{n_N} |0_{\text{tc}}\rangle$ , gives the fermion Hamiltonian

$$\hat{H}_\psi(t) = \langle \vec{n}^e | \hat{H}_{\text{tc}} + \hat{H}_d(t) | \vec{n}^e \rangle \quad (\text{S20})$$

$$= \sum_p \left\{ g i \hat{\gamma}_p \hat{\gamma}'_p + f_x(t) i \hat{\gamma}_p \hat{\gamma}'_{p+x} \right. \quad (\text{S21})$$

$$\left. + f_y(t) \hat{S}_p^{(y)} i \hat{\gamma}_p \hat{\gamma}'_{p+y} \right\} \quad (\text{S22})$$

Re-expressing the Majorana operators in terms of complex fermions  $\hat{f}_p$  and  $\hat{f}_p^\dagger$  via Eq. (S13), defining the fermion chemical potential  $\mu_\psi = g$  and neglecting constant energy shifts then gives the fermion Hamiltonian of Eq. (4) of the main text.

Consider now  $e$ -boson (vortex) movement. This is induced by the single-spin operator  $\hat{Z}_i$ . In the quasiparticle mapping, for spins in the bulk, this is mapped to

$$\begin{aligned} \hat{Z}_{v,R} &= (\hat{b}_v^\dagger + \hat{b}_v)(\hat{b}_{v+x}^\dagger + \hat{b}_{v+x}), \\ \hat{Z}_{v,T} &= \hat{S}_v^{(y)}(\hat{b}_v^\dagger + \hat{b}_v)(\hat{b}_{v+y}^\dagger + \hat{b}_{v+y}), \end{aligned} \quad (\text{S23})$$

with

$$\hat{S}_v^{(y)} = \left[ \prod_{p \in \mathbb{L}[p(v+y)]} (-i \hat{\gamma}_p \hat{\gamma}'_p) \right]. \quad (\text{S24})$$

Hence, horizontal tunnelling has ‘no strings attached’, while vertical vortex tunnelling carries a string of fermion parities spanning over all the plaquettes to the left of the bond connecting vertices  $v$  and  $v+y$ .

## FLOQUET ENGINEERING

In this section, the high-frequency effective Hamiltonian of Eq. (5), produced by the driven Hamiltonian  $\hat{H}_\psi(t)$  of Eq. (3), is derived.

Following Floquet’s Theorem, the evolution operator generated at time  $t$  by the time-periodic  $\hat{H}_\psi(t) = \hat{H}_\psi(t+T)$ , starting from initial time  $t_0$ , can be decomposed according to [27]

$$\hat{U}(t) = \hat{K}(t) e^{-i\hat{H}_F(t-t_0)} \hat{K}^\dagger(t_0), \quad (\text{S25})$$

in terms of an effective time-independent Floquet Hamiltonian  $\hat{H}_F$  and a time-periodic micromotion operator

$\hat{K}(t) = \hat{K}(t+T) = e^{\hat{G}(t)}$ , generated by  $\hat{G}(t)$ . Both  $\hat{H}_F$  and  $\hat{G}(t)$  can be determined order by order in a high-frequency expansion in powers of  $\omega^{-n}$  [25, 30]. The leading order is given by

$$\hat{H}_F = \hat{H}_0 = \frac{1}{T} \int_0^T \hat{H}_\psi(t) dt, \quad (\text{S26a})$$

$$\hat{G}(t) = - \sum_{m \neq 0} \frac{e^{im\omega t} \hat{H}_m}{m\omega}, \quad (\text{S26b})$$

where we have indicated the Fourier components of  $\hat{H}_\psi(t)$  with

$$\hat{H}_m = \frac{1}{T} \int_0^T dt \hat{H}_\psi(t) e^{-im\omega t}. \quad (\text{S27})$$

To compute the expansion, we first represent the Hamiltonian  $\hat{H}_\psi(t)$  in a rotating frame defined by the gauge transformation

$$\hat{R}(t) = \exp \left( -it \frac{\omega}{2} \sum_p \hat{f}_p^\dagger \hat{f}_p \right). \quad (\text{S28})$$

At the end of the period,  $\hat{R}(T)$  reduces to the total fermion parity of the system,  $\hat{R}(T) = \exp(-i\pi \sum_p \hat{f}_p^\dagger \hat{f}_p)$ . Since the latter is a conserved quantity,  $\hat{R}(t)$  commutes with the Floquet Hamiltonian,  $[\hat{R}(t), \hat{H}_F] = 0$ . Moreover, it acts trivially within the physical subspace of even-parity states, and thus only contributes to their micromotion dynamics. The transformed Hamiltonian  $\hat{H}'_\psi(t) = \hat{R}^\dagger(t) \hat{H}_\psi(t) \hat{R}(t) - i\hat{R}^\dagger \partial_t \hat{R}(t)$  reads

$$\begin{aligned} \hat{H}'_\psi(t) &= \sum_p \left[ (\mu_\psi - \omega/2) \hat{f}_p^\dagger \hat{f}_p \right. \\ &\left. + \sum_{r \in \{x,y\}} d_r(t) \hat{S}_p^{(r)} (e^{i\omega t} \hat{f}_p \hat{f}_{p+r} + \hat{f}_p^\dagger \hat{f}_{p+r}^\dagger + \text{H.c.}) \right]. \end{aligned} \quad (\text{S29})$$

Inserting the drive  $d_r(t)$  of Eq. (4) gives

$$\begin{aligned} \hat{H}'_\psi(t) &= \sum_p \left\{ (\mu_\psi - \omega/2) \hat{f}_p^\dagger \hat{f}_p \right. \\ &- \sum_{r \in \{x,y\}} \hat{S}_p^{(r)} J (e^{i\omega t} \hat{f}_p \hat{f}_{p+r} + \hat{f}_p^\dagger \hat{f}_{p+r}^\dagger + \text{H.c.}) \\ &- \sum_{r \in \{x,y\}} \hat{S}_p^{(r)} \Delta [e^{i\phi_r} (\hat{f}_p \hat{f}_{p+r} + e^{i\omega t} (\hat{f}_p^\dagger \hat{f}_{p+r}^\dagger + \hat{f}_{p+r}^\dagger \hat{f}_p)) \\ &\left. + e^{i2\omega t} \hat{f}_p \hat{f}_{p+r} + \text{H.c.}] \right\}. \end{aligned} \quad (\text{S30})$$

Computing the time average as per Eq. (S26a) yields the time independent part of Eq. (S30),

$$\begin{aligned} \hat{H}_0 &= \sum_p \left\{ -\mu \hat{f}_p^\dagger \hat{f}_p - \sum_{r \in \{x,y\}} \hat{S}_p^{(r)} (J \hat{f}_p^\dagger \hat{f}_{p+r} \right. \\ &\left. + \Delta e^{i\phi_r} \hat{f}_p \hat{f}_{p+r} + \text{H.c.}) \right\}, \end{aligned} \quad (\text{S31})$$

where we have defined the effective chemical potential  $\mu = -(\mu_\psi - \pi/T)$ . The kick operator  $\hat{G}(t)$  to leading order is determined by Eq. (S26b), by  $\hat{R}(t)$  and by the Fourier components of  $\hat{H}'_\psi(t)$ , which from Eq. (S30) read

$$\begin{aligned} \hat{H}'_1 = & - \sum_p \sum_{r \in \{x,y\}} \hat{S}_p^{(r)} J \hat{f}_p \hat{f}_{p+r} \\ & - \sum_p \sum_{r \in \{x,y\}} \hat{S}_p^{(r)} \Delta e^{i\phi_r} (\hat{f}_p^\dagger \hat{f}_{p+r} + \hat{f}_{p+r}^\dagger \hat{f}_p), \end{aligned} \quad (\text{S32})$$

$$\begin{aligned} \hat{H}'_{-1} = & - \sum_p \sum_{r \in \{x,y\}} \hat{S}_p^{(r)} J \hat{f}_{p+r}^\dagger \hat{f}_p^\dagger \\ & - \sum_p \sum_{r \in \{x,y\}} \hat{S}_p^{(r)} \Delta e^{-i\phi_r} (\hat{f}_p^\dagger \hat{f}_{p+r} + \hat{f}_{p+r}^\dagger \hat{f}_p), \end{aligned} \quad (\text{S33})$$

$$\hat{H}'_2 = - \sum_p \sum_{r \in \{x,y\}} \hat{S}_p^{(r)} \Delta e^{i\phi_r} \hat{f}_p \hat{f}_{p+r}, \quad (\text{S34})$$

$$\hat{H}'_{-2} = - \sum_p \sum_{r \in \{x,y\}} \hat{S}_p^{(r)} \Delta e^{-i\phi_r} \hat{f}_{p+r}^\dagger \hat{f}_p^\dagger. \quad (\text{S35})$$

## APPENDIX: EXCHANGE PHASES

### Bogoliubov-de Gennes quasiparticles.

In this section, we discuss how the Floquet-BCS ground state of the Floquet Hamiltonian is constructed and used to compute geometric phases when vortices are displaced. The fermion Floquet Hamiltonian takes the general form

$$\hat{H} = - \sum_j \mu_j n_j - \sum_{\langle ij \rangle} (J_{ij} \hat{f}_i^\dagger \hat{f}_j + \Delta_{ij}^* \hat{f}_i \hat{f}_j + \text{H.c.}) \quad (\text{S36})$$

and can be expressed as  $\hat{H} = (1/2)(\hat{\mathbf{f}}^\dagger, \hat{\mathbf{f}}) \hat{H}_{\text{BdG}}(\hat{\mathbf{f}}, \hat{\mathbf{f}}^\dagger)^T$  in terms of the Bogoliubov-de Gennes Hamiltonian  $\hat{H}_{\text{BdG}}$ . Diagonalizing the BdG Hamiltonian,

$$\hat{H}_{\text{BdG}} \begin{pmatrix} \mathbf{u}_n \\ \mathbf{v}_n \end{pmatrix} = E_n \begin{pmatrix} \mathbf{u}_n \\ \mathbf{v}_n \end{pmatrix} \quad (\text{S37})$$

$$\hat{H}_{\text{BdG}} \begin{pmatrix} \mp \mathbf{v}_n^* \\ \mathbf{u}_n^* \end{pmatrix} = -E_n \begin{pmatrix} \mp \mathbf{v}_n^* \\ \mathbf{u}_n^* \end{pmatrix}, \quad (\text{S38})$$

gives pairs of particle-hole symmetric energies  $\pm E_n$  and eigenvectors. One can use them to construct quasiparticle operators  $\hat{\alpha}_n$ ,

$$\begin{pmatrix} \hat{\alpha}_1 \\ \vdots \\ \hat{\alpha}_N \\ \hat{\alpha}_1^\dagger \\ \vdots \\ \hat{\alpha}_N^\dagger \end{pmatrix} = \begin{bmatrix} \mathbf{u}_1^{*,T} & \mathbf{v}_1^{*,T} \\ \vdots & \vdots \\ \mathbf{u}_N^{*,T} & \mathbf{v}_N^{*,T} \\ \mathbf{v}_1^T & \mathbf{u}_1^T \\ \vdots & \vdots \\ \mathbf{v}_N^T & \mathbf{u}_N^T \end{bmatrix} \begin{pmatrix} \hat{f}_1 \\ \vdots \\ \hat{f}_N \\ \hat{f}_1^\dagger \\ \vdots \\ \hat{f}_N^\dagger \end{pmatrix} = \hat{U}^\dagger \begin{pmatrix} \mathbf{f} \\ \mathbf{f}^\dagger \end{pmatrix}, \quad (\text{S39})$$

where  $\hat{U}$  is of the form

$$\hat{U} = \begin{pmatrix} u & v^* \\ v & u^* \end{pmatrix}, \quad (\text{S40})$$

such that  $\hat{H}$  is brought to canonical form

$$\hat{H} = E_{\text{GS}} + \sum_{n=1}^N E_n \hat{\alpha}_n^\dagger \hat{\alpha}_n, \quad (\text{S41})$$

with ground state energy

$$E_{\text{GS}} = -\frac{1}{2} \sum_{n=1}^N E_n. \quad (\text{S42})$$

The ground state  $|\Phi\rangle$  is determined by the condition of being annihilated by all quasiparticle operators,  $\hat{\alpha}_n |\Phi\rangle = 0$ . It can be written explicitly in generalized BCS form [48],

$$|\Phi\rangle = \mathcal{N} \exp \left( \frac{1}{2} \sum_{ij} T_{ij} \hat{f}_i^\dagger \hat{f}_j^\dagger \right) |0\rangle, \quad (\text{S43})$$

with a Thouless matrix  $T_{ij}$ , with respect to the chosen reference state  $|0_{\text{tc}}\rangle$ , which is the fermion vacuum. The normalization constant is  $\mathcal{N} = \sqrt{\det(u)}$ , with  $u$  defined in Eq. (S40). In case  $|\Phi\rangle$  has vanishing overlap with the fermion vacuum,  $\langle \Phi | 0_{\text{tc}} \rangle = 0$ , a different reference state needs to be chosen, as also further discussed below. By imposing  $\hat{\alpha}_n |\Phi\rangle = 0$ , the Thouless matrix  $T_{ij}$  is found as  $T = -(u^*)^{-1} v^*$  [48]. Since, for the toric-code model on a torus, only pairs of fermionic quasiparticles can be created or annihilated, the physical states must have even fermionic parity. The ground state parity is determined by the BdG Hamiltonian and is computed following Ref. [8].

In case the lowest energy state of  $\hat{H}_{\text{BdG}}$  has odd parity, the physical ground state will be the one containing the first BdG quasiparticle. This can be determined as the state which is annihilated by all the operators  $\alpha_j$  with  $j \neq 1$  and by  $\alpha_j^\dagger$  [21, 48].

**Geometric phase.** To compute the geometric phase accumulated by moving a vortex along a given path, we follow the strategy of Refs. [21, 45], adapted here to the Floquet system. We consider controlled vortex movement within the bulk, that never spans the whole lattice, such that no flipping of the eigenvalues of the Wilson loop operators (change of superselection sector) can occur. For each position of the vortices along the path, the fermion Floquet-BCS corresponding to that vortex configuration is computed from the BdG Hamiltonian as explained in the previous section, resulting in a sequence of fermion ground states  $|\Phi_j\rangle$ . To avoid dependence of the phase from the details of the exchange path, Levin-Wen's protocol [45] is employed, which requires one to

compute the difference  $\theta = \theta_P - \theta_{P'}$  of the phases  $\theta_P$  accumulated along two  $T$ -shape paths depicted in Fig. 3(a). The phase along path  $P$  is computed as

$$\theta_P = \text{Arg} \prod_{(i,i+1) \in P} \langle \Phi_{i+1} | \hat{t}_{i+1,i} | \Phi_i \rangle \quad (\text{S44})$$

Here, the operator  $\hat{t}_{i,j}$  represents the fermionic part of the  $e$ -boson tunnelling operators of Eq. (S23) which converts the vortex spatial configuration  $|\vec{n}_j^e\rangle$ , associated with the fermion BCS ground state  $|\Phi_j\rangle$ , into  $|\vec{n}_j^e\rangle$ , associated with  $|\Phi_i\rangle$ . In the quasiparticle picture,  $\hat{t}_{i,j}$  is given by the string  $\hat{\mathcal{S}}_p^{(y)}$  of fermion parities of Eq. (S24). Hence, the matrix elements in Eq. (S44) reduce, for horizontal vortex displacement, to computing the overlap between ‘neighbouring’ BCS wavefunctions, while, for vertical displacement, one needs to compute matrix elements of the form

$$\langle \Phi_{i+1} | \hat{\mathcal{S}}_p^{(y)} | \Phi_i \rangle. \quad (\text{S45})$$

To compute overlaps, we choose  $|\Phi_1\rangle$  as a reference state to construct all other Floquet BCS ground states  $|\Phi_\ell\rangle$ , rather than the bare fermion vacuum as in Eq. (S43), according to

$$|\Phi_\ell\rangle = \mathcal{N}_\ell \exp \left( \frac{1}{2} \sum_{i,j} T_{ij}^{(\ell)} \alpha_{\ell,i}^\dagger \alpha_{\ell,j}^\dagger \right) |\Phi_1\rangle. \quad (\text{S46})$$

On the one hand, this choice of reference state ‘saves’ one computation step by fixing the phase in the first step to  $\text{Arg}\langle \Phi_2 | \Phi_1 \rangle = 0$ , since the ansatz of Eq. (S46) implicitly fixes the gauge along the path through the condition that  $\langle \Phi_i | \Phi_1 \rangle = \mathcal{N}_1$  is real. On the other, it is a convenient choice since  $\langle \Phi_i | \Phi_1 \rangle$  typically remains fairly large, avoiding numerical issues in the construction of the state associated with small overlaps.

The Thouless matrix  $T_{ij}^{(\ell)}$  and operators  $\hat{\alpha}_\ell$  can be determined by using the eigenvectors of the 1st and  $\ell$ th Floquet-BdG Hamiltonians, which give rise to the two sets of quasiparticle operators

$$\begin{pmatrix} \hat{\alpha}_1 \\ \hat{\alpha}_1^\dagger \end{pmatrix} = \hat{U}_1^\dagger \begin{pmatrix} \hat{f} \\ \hat{f}^\dagger \end{pmatrix}, \quad \begin{pmatrix} \alpha_\ell \\ \alpha_\ell^\dagger \end{pmatrix} = \hat{U}_\ell^\dagger \begin{pmatrix} \hat{f} \\ \hat{f}^\dagger \end{pmatrix}, \quad (\text{S47})$$

respectively, where  $\hat{U}_\ell$  have the form of Eq. (S40) in terms of submatrices  $u_\ell$  and  $v_\ell$ . The matrix  $T^{(\ell)}$  is then given

by  $T^{(\ell)} = -(\tilde{u}_\ell^*)^{-1} \tilde{v}_\ell^*$ , where the matrices  $\tilde{u}_\ell$  and  $\tilde{v}_\ell$  are defined by [48]

$$\tilde{u}_\ell = u_1^\dagger u_\ell + v_1^\dagger v_\ell, \quad (\text{S48a})$$

$$\tilde{v}_\ell = v_1^T u_\ell + u_1^T v_\ell. \quad (\text{S48b})$$

Given two ground states  $|\Phi_i\rangle$  and  $|\Phi_j\rangle$ , characterized by Thouless matrices  $T^{(i)}$  and  $T^{(j)}$ , their overlap can be computed according to [49]

$$\langle \Phi_i | \Phi_j \rangle = (-1)^{N(N+1)/2} \text{pf} \begin{pmatrix} T^{(j)} & -\mathbf{1} \\ \mathbf{1} & -T^{(i),*} \end{pmatrix}, \quad (\text{S49})$$

where  $\text{pf}(\cdot)$  denotes the Pfaffian. To compute the matrix elements of Eq. (S45), we note that, if  $|\Phi\rangle$  is the quasiparticle vacuum associated with the BdG Hamiltonian  $\hat{H}_{\text{BdG}}$ , then  $|\Phi'\rangle = \hat{Q}^\dagger |\Phi\rangle$  with  $\hat{Q}$  unitary is a quasiparticle vacuum associated with the transformed BdG Hamiltonian

$$\hat{H}'_{\text{BdG}} = \hat{Q}^\dagger \hat{H}_{\text{BdG}} \hat{Q}. \quad (\text{S50})$$

Given the matrix  $\hat{U}$  of eigenvectors of  $\hat{H}_{\text{BdG}}$ , the matrix  $\hat{U}'$  of eigenvectors of  $\hat{H}'_{\text{BdG}}$  is then  $\hat{U}' = \hat{Q}^\dagger \hat{U}$ . The latter can then be used to construct the representation of the BCS vacuum  $|\Phi'\rangle$  with respect to the reference state  $|\Phi_1\rangle$  according to Eq. (S46) and (S48) and then be used to compute its overlap with  $|\Phi\rangle$  via Eq. (S49). However, there is an additional caveat. Using the representation (S46) fixes the gauge of  $|\Phi'\rangle$  by imposing a real  $\langle \Phi' | \Phi_1 \rangle$ , which is unwanted. Indeed, consistency with the gauge choice made along the path,  $\langle \Phi_i | \Phi_1 \rangle \in \mathbb{R}$ , only requests that each ground state  $|\Phi\rangle$  (and not also  $\hat{Q} |\Phi\rangle$ ) has real overlap with the reference state  $|\Phi_1\rangle$ . To remedy for this, in the computation of the phase in Eq. (S45) we introduce a fictitious intermediate step to  $|\Phi_i\rangle$  to fix the gauge choice, namely

$$\langle \Phi_j | \hat{Q} | \Phi_i \rangle \longrightarrow \langle \Phi_j | \Phi'_i \rangle \langle \Phi'_i | \Phi_i \rangle. \quad (\text{S51})$$

To see that this re-establishes the correct phase, note that  $|\Phi'\rangle$  is equal to  $\hat{Q} |\Phi\rangle$  up to some phase  $\theta$ ,  $|\Phi'\rangle = e^{i\theta} \hat{Q} |\Phi\rangle$ . Inserting the latter expression into Eq. (S51), one obtains that the phase  $\theta$  cancels out, leaving

$$\langle \Phi_j | \Phi'_i \rangle \langle \Phi'_i | \Phi_i \rangle = \langle \Phi_j | \hat{Q} | \Phi_i \rangle \langle \Phi_i | \hat{Q} | \Phi_i \rangle. \quad (\text{S52})$$

If  $\hat{Q}$  is Hermitian, as  $\hat{\mathcal{S}}_p^{(y)}$  of Eq. (S45) is, the diagonal element  $\langle \Phi_i | \hat{Q} | \Phi_i \rangle$  is real, and thus the phase contribution in Eq. (S52) only comes from  $\langle \Phi_j | P | \Phi_i \rangle$  as desired.